Importance of interorbital charge transfers for the metal-to-insulator transition of BaVS$_3$

Frank Lechermann,[1,2] Silke Biermann,[1,3] and Antoine Georges[1,3]

^{1}CPHT École Polytechnique, 91128 Palaiseau Cedex, France
^{2}LPT-ENS, 24 Rue Lhomond, 75231 Paris Cedex 05, France
^{3}Laboratoire de Physique des Solides, CNRS-UMR 8502, UPS Bâtiment 510, 91405 Orsay, France

The underlying mechanism of the metal-to-insulator transition (MIT) in BaVS$_3$ is investigated, using dynamical mean-field theory in combination with density functional theory. It is shown that correlation effects are responsible for a strong charge redistribution, which lowers the occupancy of the broader A_{1g} band in favor of the narrower E_g bands. This resolves several discrepancies between band theory and the experimental findings, such as the observed value of the charge-density wave ordering vector associated with the MIT, and the presence of local moments in the metallic phase.

PACS numbers: 71.30.+h, 71.15.Mb, 71.10.Fd, 75.30.Cr

The structural, electronic and magnetic properties of the vanadium sulphide compound BaVS$_3$ raise several puzzling questions [1, 2]. At room temperature, this material crystallizes in a hexagonal ($P6_3/mmc$) structure [3], in which straight chains of face-sharing VS$_6$ octahedra are directed along the c-axis. At $T_s \sim 240$ K the crystal structure transforms into an orthorhombic ($Cmc2_1$) structure [4], thereby creating an anisotropy in the ab-plane (i.e., perpendicular to the chain direction) and a zigzag distortion of the VS$_3$ chains in the bc-plane. Additionally, the Hall coefficient changes sign from negative to positve at T_s [2]. On further cooling the system displays a metal-to-insulator transition (MIT) at $T_{\mathrm{MIT}} \sim 70$ K. Remarkably, this transition is second-order and is not accompanied by magnetic ordering. Only below $T_X \sim 30$ K indications for an incommensurate antiferromagnetic order exist [5].

Forró et al. [6] have found that the MIT can be driven to $T=0$ by applying pressure [7]. Further recent experiments [8, 9] have demonstrated that the MIT is in fact associated with a structural transition. These studies establish that a commensurate structural modulation sets in, corresponding to a reduced wave vector $\mathbf{q}=(1,0,\frac{1}{2})_O$ in the orthorhombic cell. Furthermore, the X-ray diffuse scattering experiments of Fagot et al. [9] reveal a large fluctuation regime with critical wave vector $q_c=0.5c^*$ (here c^* is the reciprocal unit vector along the c-axis of the orthorhombic system), extending up to 170 K into the metallic phase. In the same temperature range the Hall coefficient is strongly increasing [2]. This regime might be interpreted as a precursor of the charge density wave (CDW) instability, reminiscent of the large fluctuations in a quasi one-dimensional (1D) metal in the vicinity of a Peierls transition. It should be kept in mind however that the conduction anisotropy within the system is not strongly pronounced ($\sigma_c/\sigma_a \sim 3$-4) [10], making 1D interpretations questionable. The "metallic" phase above T_{MIT} displays several other unusual properties [7, 10]. The resistivity is rather high (a few mΩcm) and metallic-like ($d\rho/dT>0$) only above ~ 150 K. It dis-

plays a weak minimum at this temperature, below which it increases upon further cooling. Most interestingly, this phase displays local moments, as revealed by the Curie-Weiss form of the magnetic susceptibility. The effective moment corresponds approximately to one localized spin-1/2 per two V sites. Since the formal valence is V^{4+}, corresponding to one electron in the $3d$-shell, this can be interpreted as the effective localization of half of the electrons. At T_{MIT}, the susceptibility rapidly drops, and the electronic entropy is strongly suppressed [11].

In the hexagonal high-T phase the low-lying V($3d$) levels consist of an A_{1g} state and two degenerate E_g states. A further splitting of the degenerate states occurs in the orthorhombic phase. First-principles calculations of the electronic structure of BaVS$_3$, based on density functional theory (DFT) in the local (spin) density approximation (L(S)DA), have been performed in Refs. [12, 13, 14]. For both phases, the calculations do yield a V($3d$)-S($3p$) hybridization which is strong enough to account for the weak anisotropy of the transport properties. No band-gap opening has been reached within L(S)DA. Instead, very narrow E_g bands right at the Fermi level, and a nearly filled dispersive band with mainly A_{1g} character extending along the c^* direction have been found. This is consistent with a simple model proposed early on by Massenet et al. [15]. However, the occupancy of the narrow E_g bands found within LDA is too low to account for the observed local moment in the metallic phase. The nature of the CDW instability is also left unexplained by the DFT calculations. Indeed, the calculated value of the Fermi wave vector of the broad A_{1g} band is found to be $2k_F^{\mathrm{LDA}} \simeq 0.94c^*$ [13], while the observed wave vector of the instability is $q_c=0.5c^*$ [9]. Therefore, the simple picture of a CDW at $q_c=2k_F$ associated only with the A_{1g} band is untenable within LDA. It is likely that the E_g states also participate in the instability, but the LDA band structure does not provide a Fermi-surface nesting compatible with the experimental q value [1]. Hence, ab-initio calculations based on L(S)DA are not sufficient to explain the electronic struc-
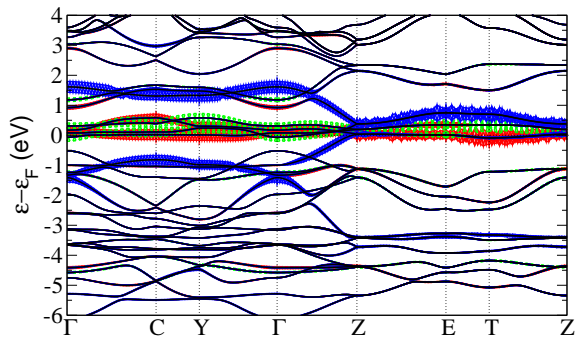
FIG. 1: LDA band structure for BaVS$_3$ in the $Cmc2_1$ structure. Also shown are the fatbands (see text) for the A_{1g} (blue/full dark), E_{g1} (red/full grey) and E_{g2} (green/dashed grey) orbital of the V atoms.
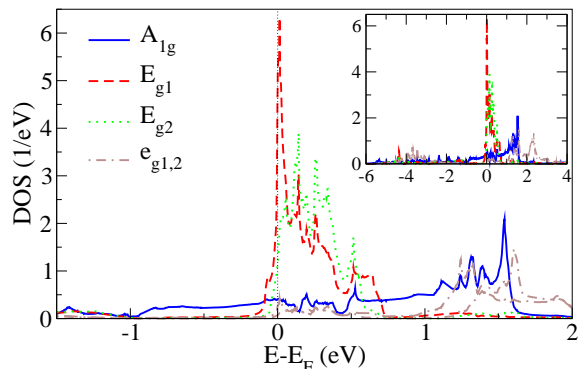

FIG. 2: Angular momentum-resolved LDA-DOS of the symmetry-adapted V(3d) states.

ture of BaVS$_3$. By using static DFT+U schemes a band gap was obtained [16]. However, this required to enforce magnetic order, hence leaving the question of the mechanism of the transition into the paramagnetic insulator unanswered [24].

In this letter, we present calculations in the framework of dynamical mean field theory (DMFT), using the LDA electronic structure as a starting point. On the basis of this LDA+DMFT treatment we propose correlation effects in a multi-orbital context as an explanation for the discrepancies between band theory predictions and experiments. Specifically, we show that interorbital charge transfers occur, driven by the on-site Hund's coupling. This lowers the occupancy of the A_{1g} orbital in favor of the E_g's, hence shifting $k_F(A_{1g})$ towards lower values. From a calculation of the local susceptibilities, we demonstrate that local moments are formed in the metallic phase, due to the low quasiparticle coherence scale induced by the strong correlations (particularly for the narrow E_g bands).

On Fig. 1 the band structure of BaVS$_3$ calculated within LDA for the T=100 K orthorhombic ($Cmc2_1$) crystal structure [4] is displayed. The calculations were performed by using norm-conserving pseudopotentials

and a mixed basis consisting of plane waves and localized functions [17]. The results are consistent with previous work [12, 13, 14]. The symmetry-adapted V(3d)-basis $\{\phi_m\}$ was obtained by diagonalising the orbital density matrix $n_{MM'} \sim \sum_{\mathbf{k}b} f_{\mathbf{k}}^b \langle \psi_{\mathbf{k}}^b | M \rangle \langle M' | \psi_{\mathbf{k}}^b \rangle$, where $\psi_{\mathbf{k}}^b$ stands for the pseudo crystal wave function for wave vector $\mathbf{k}$ and band b, and M, M' denote the cubic harmonics for l=2. Being directed along the chain direction between pairs of V atoms, the A_{1g} orbital has mainly d_{z^2} character. In contrast, the E_g states, linear combinations of d_{yz}, $d_{x^2-y^2}$ and d_{z^2} (E_{g1}) as well as d_{xy} and d_{xz} (E_{g2}), only weakly hybridize with their surrounding. The orbitals of the remaining e_g manifold point mainly towards the sulphur atoms, which results in a large energy splitting, leading to a smaller(larger) contribution to the occupied(unoccupied) states well below(above) ε_F. Hence, the e_g states do not have a major influence on the essential physics around the MIT. Note that in the orthorhombic structure (as already in the hexagonal one), the unit-cell contains two formula units, with the two V-sites equivalent by symmetry. The high-symmetry points Γ-C-Y in the Brillouin Zone (BZ) define a triangle in the k_z=0 plane, whereas Z-E-T is the analogous shifted triangle in the k_z=0.5c^* plane. The Γ-Z line corresponds to the propagation along the c-axis. We have used a "fatband" representation associated with the $\{A_{1g}, E_g\}$ orbitals on Fig. 1 in which the width is proportional to the amount of orbital character of each band at a given k-point. Thus, one can identify that the narrow bands at the Fermi level are associated with the E_g orbitals. Along Γ-Z starting at around -1 eV, one observes the dispersive band with strong A_{1g} character that crosses ε_F close to the edge of the BZ. Hence the Γ-Z portion of that band is almost filled, with $2k_F \simeq 0.94c^*$ as mentioned above. The E_{g2} electron pocket at the Γ-point is absent for the hexagonal high-T structure (see also [13]). Its existence might be related to the hole-like transport below T_S as revealed from Hall measurements [2]. The partial density of states (DOS) for each orbital displayed on Fig. 2, show a rather broad A_{1g} DOS while the E_g's yield very narrow peaks right at and above E_F.

Recently, it has become possible to investigate correlation effects in a realistic setting by combining LDA with DMFT [18, 19]. Starting from the LDA hamiltonian $H_{mm'}^{\mathrm{LDA}}(\mathbf{k})$ expressed in a localized basis set, many-body terms are introduced, leading to a self-energy matrix $\Sigma_{mm'}$ which is taken to be local ($\mathbf{k}$-independent) but fully frequency-dependent. In the present work, we use a simplified implementation of the LDA+DMFT approach, which is geared at keeping those physical ingredients which are important for the physics of BaVS$_3$ close to the MIT. Specifically, we work within an effective 3-band model, whereby the LDA electronic structure enters via the DOS in the relevant energy window around the Fermi level. The effective bands are derived from the symmetry-adapted $\{A_{1g}, E_g\}$ states, thus non-diagonal
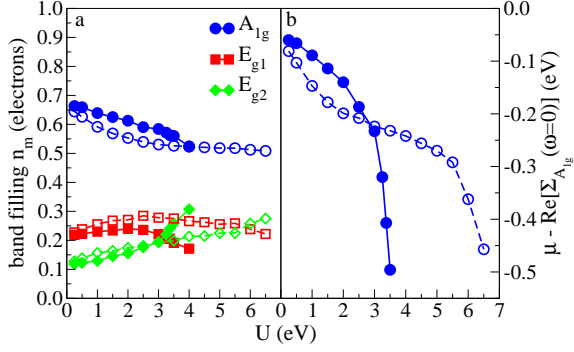
FIG. 3: (a) Band fillings at $\beta=(k_\mathrm{B}T)^{-1}=15$ eV^{-1} (T=774 K) for the effective bands within LDA+DMFT. (b) Corresponding shift of the Fermi level for the A_{1g} band (note that $\varepsilon_{\mathbf{k}_F}^{(\mathrm{LDA})}=0$). Filled symbols: U/J=7, open symbols: U/J=4.

FIG. 4: LDA+DMFT spectral data for U=3.5 eV, U/J=4. (a) V($3d$) low-energy quasiparticle bands along Γ-Z in LDA (dashed lines) and LDA+DMFT (solid lines) for T=332 K. (b,c) integrated spectral function $\rho(\omega)$ for a single formula unit of BaVS$_3$ at T=1160 K (b) and T=332 K (c).

self-energy terms $\Sigma_{m\neq m'}$ are negligible. A physically adequate 'empirical downfolding' procedure was used in order to construct the effective 3-band DOS. First, we took care of the $3d^1$ character. The location and width ($\sim$2.2 eV) of the energy window were chosen such that the total DOS accomodates two electrons below and ten electrons above the Fermi level (per two V). Since the e_g bands are hardly relevant and of minor weight close to E_F, they were hybridized with the E_g bands as suggested from the resolved partial DOS on Fig. 2. The contribution of these new E_g bands was substracted from the total DOS normalized to a single formula unit of BaVS$_3$ within the chosen energy window. The resulting difference was identified as the new downfolded A_{1g} band, since the A_{1g} orbital substantially hybridizes with the S($3p$) orbitals. Finally, the self-energies Σ_m associated with these effective bands are calculated from LDA+DMFT where the self-consistency condition is expressed as an integral over the effective partial DOS $D_m^{\mathrm{LDA}}(\varepsilon)$. The on-site interaction matrix was parametrised as: $U_{mm}^{\uparrow\downarrow}=U$, $U_{m\neq m'}^{\uparrow\downarrow}=U-2J$ and $U_{m\neq m'}^{\uparrow\uparrow(\downarrow\downarrow)}=U-3J$, with U the on-site Coulomb repulsion and J the local Hund's rule coupling. The DMFT local impurity problem was solved using the quantum Monte-Carlo (QMC) Hirsch-Fye algorithm. Up to 128 slices in imaginary time τ and at most 10^6 sweeps were used [25].

Fig. 3a displays our results for the occupancies of each orbital, as a function of U. In the absence of a precise determination of this parameter from either experiments (e.g., photoemission) or theory (constrained LDA methods tend to underestimate the screening for metals), we varied U over a rather large range of values. The ratio U/J was chosen to be fixed, and two series were studied: U/J=7 and U/J=4, corresponding to a weaker and stronger Hund's coupling, respectively. The orbital occupancies in our effective 3-band model, at the LDA level (i.e., for U=0) read: $n(A_{1g})$=0.712, $n(E_{g1})$=0.207 and $n(E_{g2})$=0.081. The main effect apparent on Fig. 3a is
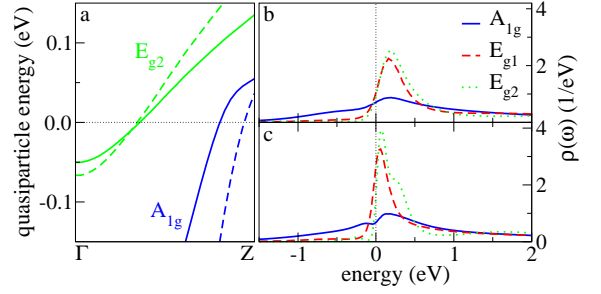
that moderate correlations tend to bring the occupancies of each orbital closer to one another, i.e., to decrease the population of the "extended" orbital A_{1g} and to increase the occupancy of each E_g orbital. For strong correlations, values close to $n(A_{1g})\simeq n(E_{g1})+n(E_{g2})\simeq$0.5 are obtained in the DMFT calculation, corresponding to a half-filled band. In the absence of correlations, it pays to occupy dominantly the broad A_{1g} band, which provides the largest kinetic energy gain, while in the presence of correlations this has to be balanced versus the potential energy cost. The Hund's coupling clearly favors such an interorbital charge redistribution, as also pointed out recently in the context of ruthenates [20]. For larger U, band-narrowing effects reduce the kinetic energy of the A_{1g} band, hence also reducing its occupancy [21] in favor of E_g. As expected, a Mott insulating state is obtained when U is increased beyond a critical value, which is found to depend strongly on J (the range of U's displayed in Fig. 3 corresponds to the metallic regime for each series, on which we focus in this paper).

Our calculations reveal that the depletion of the A_{1g} band is accompanied by a reduction of the corresponding k_F along the Γ-Z direction. (Note that the Luttinger theorem [22] does not apply separately for each band but only relates the total Fermi surface volume to the total occupancy). While a full determination of the quasiparticle (QP) band structure in the interacting system requires a determination of the real-frequency self-energy, we can extract the low-energy expansion of this quantity from our QMC calculation, in the form: $\mathrm{Re}\Sigma_m(\omega+i0^+)\simeq\mathrm{Re}\Sigma_m(0)+\omega(1-1/Z_m)+\cdots$, with Z_m the QP residue associated with each orbital. The poles of the Green's function determine the QP dispersion relation: $\det[\omega_\mathbf{k}-\hat{Z}[\hat{H}_\mathbf{k}^{\mathrm{LDA}}+\mathrm{Re}\hat{\Sigma}(0)-\mu]]$=0, with μ the chemical potential. Focusing first on the A_{1g} sheet of the Fermi surface, within our diagonal formulation the location of the Fermi wave vector in the interacting system is determined by: $\varepsilon_{A_{1g}}^{\mathrm{LDA}}(\mathbf{k}_F)=\mu-\mathrm{Re}\Sigma_{A_{1g}}(0)$. This quantity therefore yields the energy shift of the A_{1g} band
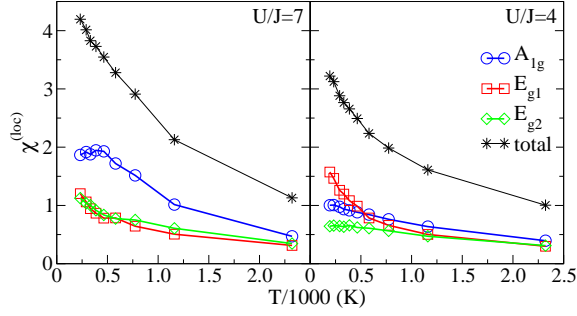
FIG. 5: T-dependent local spin susceptibilities for U=3.5 eV, according to the normalization $\chi^{(\text{loc})}=\int_0^\beta d\tau \langle \hat{S}_z(0)\hat{S}_z(\tau)\rangle$, where $\hat{S}_z$ denotes the z-component of the spin operator.

at the Fermi surface crossing, as compared to LDA. It is depicted in Fig. 3b as a function of U. On Fig. 4a, we display (for U=3.5eV and U/J=4) the QP bands that cross the Fermi level along Γ-Z in a narrow energy range around ε_F. The QP bands are obtained by performing a perturbative expansion of the pole equation above, which yields: $\omega_{b\mathbf{k}}=\sum_m C^b_{m\mathbf{k}} Z_m [\varepsilon^{\text{LDA}}_{b\mathbf{k}}+\text{Re}\Sigma_m(0)-\mu]$ with $C^b_{m\mathbf{k}}\equiv|\langle\psi^b_{\mathbf{k}}|\phi_m\rangle|^2$ the LDA orbital weight. From these two figures, it is clear that $k_F(A_{1g})$ is reduced in comparison to the LDA value, in line with the global charge transfer from A_{1g} to E_g. This opens new possibilities for the CDW instability, in particular for the nesting condition.

The enhanced population of the narrow E_g bands, as well as the correlation-induced reduction of its bandwidth (see Fig. 4a) provide an explanation for the local moments observed in the metallic phase. To support this, we have calculated (Fig. 5) the local susceptibility associated with each orbital $\chi^{(\text{loc})}_m \equiv \sum_{\mathbf{q}}\text{Re}[\chi_m(\mathbf{q},\omega=0)]$. For both values of U/J, the susceptibility of the A_{1g} band saturates to a Pauli-like value at low temperatures. In contrast, $\chi^{(\text{loc})}$ of the E_g orbitals strongly increases as T is lowered (except for the low-filled E_{g2} orbital at U/J=4). This is because the coherence temperature below which quasiparticles form is much lower for the E_g orbitals than for the A_{1g}. Accordingly, our calculation of the integrated spectral functions (Fig. 4b,c) reveals a strong T-dependence of the E_g QP peak. Some differences between the two series are clear from Fig. 5. For U/J=7, the system is very close to the Mott transition. Thus the A_{1g} electrons also act as local moments over part of the temperature range, while for U/J=4, the T-dependence of the total local susceptibility is almost entirely due to the E_{g1} electrons. Which of the two situations is closest to the physics of BaVS$_3$ does require further investigations, albeit some experimental indications point at the second possibility [23].

In conclusion, we have shown that charge redistributions due to correlations lower the occupancy of the broad A_{1g} band in favor of the narrow E_g's, in comparison to LDA calculations. This explains the presence of local moments in the metallic phase and paves the road towards a full understanding of the CDW instability of this material. Orbital-selective experimental probes are highly desirable in order to put to a test the conclusions of the present work. Among several outstanding questions still open are the detailed nature of the insulating phase (in particular regarding the partial suppression of local moments and the eventual magnetic ordering) as well as the remarkable suppression of T_{MIT} under pressure [6, 7].

Note added. After the completion of this work, we became aware of a recent angle-resolved photoemission study of BaVS$_3$ by S. Mitrovic *et al.* supporting our prediction of a reduced $k_F(A_{1g})$.

[1] M.-H. Whangbo, H.-J. Koo, D. Dai, and A. Villesuzanne, J. Solid State Chem. **175**, 384 (2003).
[2] C. H. Booth, E. Figueroa, J. M. Lawrence, M. F. Hundley, and J. D. Thompson, Phys. Rev. B **60**, 14852 (1999).
[3] R. Gardner, M. Vlasse, and A. Wold, Acta Crystallogr. B **25**, 781 (1969).
[4] M. Ghedira, M. Anne, J. Chenavas, M. Marezio, and F. Sayetat, Journal of Physics C Solid State Physics **19**, 6489 (1986).
[5] H. Nakamura, T. Yamasaki, S. Giri, H. Imai, M. Shiga, K. Kojima, M. Nishi, K. Kakurai, and N. Metoki, J. Phys. Soc. Jpn **69**, 2763 (2000).
[6] L. Forró, R. Gaál, H. Berger, P. Fazekas, K. Penc, I. Kézsmárki, and G. Mihály, Phys. Rev. Lett. **85**, 1938 (2000).
[7] T. Graf, D. Mandrus, J. M. Lawrence, J. D. Thompson, P. C. Canfield, S.-W. Cheong, and L. W. Rupp, Phys. Rev. B **51**, 2037 (1995).
[8] T. Inami, K. Ohwada, H. Kimura, M. Watanabe, Y. Noda, H. Nakamura, T. Yamasaki, M. Shiga, N. Ikeda, and Y. Murakami, Phys. Rev. B **66**(7), 073108 (2002).
[9] S. Fagot, P. Foury-Leylekian, S. Ravy, J. Pouget, and H. Berger, Phys. Rev. Lett. **90**(19), 196401 (2003).
[10] G. Mihály, I. Kézsmárki, F. Zámborszky, M. Miljak, K. Penc, P. Fazekas, H. Berger, and L. Forró, Phys. Rev. B **61**, 7831 (2000).
[11] H. Imai, H. Wada, and M. Shiga, J. Phys. Soc. Jpn. **65**, 3460 (1996).
[12] M. Nakamura, A. Sekiyama, H. Namatame, A. Fujimori, H. Yoshihara, T. Ohtani, A. Misu, and M. Takano, Phys. Rev. B **49**, 16191 (1994).
[13] L. Mattheiss, Solid State Commun. **93**, 791 (1995).
[14] M.-H. Whangbo, H.-J. Koo, D. Dai, and A. Villesuzanne, J. Solid State Chem. **165**, 345 (2002).
[15] O. Massenet, J. Since, J. Mercier, M. Avignon, R. Buder, and V. Nguyen, J. Phys. Chem. Solids **40**, 573 (1979).
[16] X. Jiang and G. Y. Guo, Phys. Rev. B **70**, 035110 (2004).

[17] B. Meyer, C. Elsässer, F. Lechermann, and M. Fähnle, *FORTRAN 90 Program for Mixed-Basis-Pseudopotential Calculations for Crystals*, Max-Planck-Institut für Metallforschung, Stuttgart (unpublished).

[18] V. I. Anisimov, A. I. Poteryaev, M. A. Korotin, A. O. Anokhin, and G. Kotliar, J. Phys. Cond. Matter **9**, 7359 (1997).

[19] A. I. Lichtenstein and M. I. Katsnelson, Phys. Rev. B **57**, 6884 (1998).

[20] S. Okamoto and A. J. Millis, cond-mat/0402267 (2004).

[21] A. Liebsch and A. Lichtenstein, Phys. Rev. Lett. **84**, 1591 (2000).

[22] J. Luttinger, Phys. Rev. **119**, 1153 (1960).

[23] P. Fazekas, K. Penc, H. Berger, L. Forró, S. Csonka, I. Kézsmárki, and G. Mihály, Physica B **312** (2002).

[24] Ref. [16] reported that without magnetic order, the filling of the A_{1g} band is actually further *increased*, in comparison to LDA.

[25] The QMC calculations were performed at temperatures significantly higher than the physical T_{MIT} (cf. Figs. 3-5). However, we still think that the essential physics close to T_{MIT} is captured. This is because the coherence scale for the broad A_{1g} band is already reached for elevated temperatures over most of the range of parameters that we have studied, and the crystal structure at T=100 K was used in the LDA calculations.